Surface tension and vapor-liquid phase coexistence of confined square-well fluid

Cite as: J. Chem. Phys. **126**, 024702 (2007); https://doi.org/10.1063/1.2424460
Submitted: 18 August 2006 . Accepted: 28 November 2006 . Published Online: 09 January 2007

Jayant K. Singh, and Sang Kyu Kwak

Surface tension and vapor-liquid phase coexistence of confined square-well fluid

Jayant K. Singh[a)]
Department of Chemical Engineering, Indian Institute of Technology Kanpur, Kanpur 208016, India

Sang Kyu Kwak[b)]
Division of Chemical and Biomolecular Engineering, School of Chemical and Biomedical Engineering, Nanyang Technological University, Singapore 637722, Singapore

(Received 18 August 2006; accepted 28 November 2006; published online 9 January 2007)

Phase equilibria of a square-well fluid in planar slit pores with varying slit width are investigated by applying the grand-canonical transition-matrix Monte Carlo (GC-TMMC) with the histogram-reweighting method. The wall-fluid interaction strength was varied from repulsive to attractive such that it is greater than the fluid-fluid interaction strength. The nature of the phase coexistence envelope is in agreement with that given in literature. The surface tension of the vapor-liquid interface is calculated via molecular dynamics simulations. GC-TMMC with finite size scaling is also used to calculate the surface tension. The results from molecular dynamics and GC-TMMC methods are in very good mutual agreement. The vapor-liquid surface tension, under confinement, was found to be lower than the bulk surface tension. However, with the increase of the slit width the surface tension increases. For the case of a square-well fluid in an attractive planar slit pore, the vapor-liquid surface tension exhibits a maximum with respect to wall-fluid interaction energy. We also report estimates of critical properties of confined fluids via the rectilinear diameter approach. © *2007 American Institute of Physics*. [DOI: 10.1063/1.2424460]

I. INTRODUCTION

Fluids under any types of confinement within pores which are micro- to nanometer size in dimension, regardless of geometry, exhibit minimal to significant deviations from bulk thermophysical as well as structural properties.[1,2] These unique phenomena of confined fluids have been found to be universal in nature. Consequently, the aim towards complete understanding of thermophysical properties of fluids under confinement has triggered numerous investigations, which later led to solutions of many experimental and theoretical inquiries with respect to different practical applications. A comprehensive review on recent studies on confined fluids is found in Gelb *et al.*[3] Among existing studies of confined fluids, the wall-fluid interfacial properties and the phase behavior are quantitatively the most studied. Nevertheless, more attention is needed to complete a firm establishment of interfacial studies of inhomogeneous fluids under confinement. Our main interest coheres with this premise in terms of the examination of the vapor-liquid interfacial behavior and the evaluation of the surface tension.

Due to difficulties in conducting experimental studies on the characterization of atomistic behaviors, molecular simulation is used to bridge the theories and the experimental outcomes. Often, experimentally unexpected yet promising paths to final products are found by computational methods. The rapid increase of computing power and new efficient algorithms have further enhanced the use of computational methods, and have made very complex problems solvable. These techniques find more importance for systems under nanopores as experiments are not practical in many cases. There are several approaches for the study of vapor-liquid equilibrium in a molecular simulation approach. Prominent examples include the Gibbs ensemble Monte Carlo (GEMC),[4] Gibbs-Duhem integration (GDI),[5] and *N-P-T* +test particle.[6–8] Panagiotopoulos used GEMC to obtain the phase behavior of a Lennard-Jones (LJ) fluid confined in a cylindrical boundary.[9] With same model fluid, Sarkisov and Monson used GDI to get the phase behavior in a disordered porous structure,[10] and Forsman and Woodward performed an isotension ensemble simulation to calculate the gas-liquid coexistence.[11] Smith and Vortler[12] extended GEMC to extract three phases of a square-well (SW) fluid under a bulk and hard slit-pore regions. The results of these methods yield properties of coexisting phases. However, the above mentioned methods are formulated in a way that does not put the phases in contact hence are not appropriate to capture vapor-liquid interfacial properties.

A combination of aforementioned methods was employed by Vortler and Smith to study the phase equilibria of a SW fluid under a slitlike hard pore.[13] They obtained the spreading pressure (pressure component parallel to the wall), phase coexistence, and critical properties by using the virtual parameter variation method, which is composed of the test particle insertion method[14] and Eppenga and Frenkel's[15] pressure calculation algorithm. In this study we determine the surface tension of the SW fluid in the same type of pore albeit using different techniques. Zhang *et al.*[16] recently obtained the surface tension of a LJ fluid under an attractive wall of a slitlike pore by using equilibrium molecular dy-

[a)]Electronic mail: jayantks@iitk.ac.in
[b)]Electronic mail: skkwak@ntu.edu.sg

namics (MD). They observed layering of molecules near the walls due to particle adsorption, which affects the frequency of the periodic movement of the rest of the particles between the walls. At the first determination, they found the surface tension of the LJ fluid, inclusive of wall-surface forces, under the confinement to be three orders higher than the one of liquid-vapor of bulk fluid. However, the vapor-liquid interfacial tension was not studied by the authors. With the same MD approach our results of a confined SW fluid show that, in general, the surface tension of vapor-liquid fluids decreases in the presence of the slitlike confinement.

In this work, we focus on studying the phase behavior and interfacial properties of the SW fluid under slitlike confined walls of a repulsive as well as an attractive nature. We demonstrate the capability of the grand-canonical transition-matrix Monte Carlo (GC-TMMC) to obtain not only phase equilibria but also interfacial tension for fluids (with the help of the finite size scaling formalism of Binder[17]) under slitlike confinement. To ensure the reliability of our surface tension results, we compare the finite size scaling studies with the results from MD simulations. The rest of the paper is organized as follows: In the next section we briefly describe methods used for calculating the surface tension by molecular simulation. Section III describes the details of simulation conditions applied in this work. Section IV presents the results and discussion, and we conclude in Sec. V.

II. METHODOLOGY

To obtain the surface tension of the SW fluid under a slit pore using MD, we start with the simulation box filled with molecules placed on a fcc lattice such that density is slightly higher than the coexistence liquid density. The next step is to create a slab by expanding the box in one direction perpendicular to the y axis (confined axis) while positions of particles stay still (e.g., $L_x=3L_z$). In this case, a periodic boundary condition is applied to x and z directions. Earlier, Diestler *et al.* and Diestler[18,19] have worked on the derivation of the Helmholtz potential for the confined system from the fundamental relation for an infinitesimal, reversible transformation. The potential is expressed by

$$dF = -SdT + \mu dN - p_{xx}s_y s_z ds_x - p_{yy}s_x s_z ds_y - p_{zz}s_x s_y ds_z, \tag{1}$$

where F is the Helmholtz free energy, S is the entropy, T is the temperature, μ is the chemical potential, N is the amount of the fluid, s_i's are the thickness of the fluid in the direction of i, and p_{ii} is the iith component of the pressure tensor.

The above equation can be written in terms of surface tensions as shown by Diestler *et al.*[18] and is given by

$$dF = -SdT + \mu dN + \gamma_1 dA + \gamma_2 A dR - p_{yy}A ds_y, \tag{2}$$

where $R=s_x/s_z$, $A=s_x s_z$, $\gamma_1=-(p_{xx}+p_{zz})s_y/2$, and $\gamma_2=(p_{zz}-p_{xx})s_y/2R$.

For a constant slit width $s_y=H$ and constant T, N, and A, we get the following expression:

$$\left(\frac{\partial F}{\partial R}\right)_{T,N,s_z,A} = \gamma_2 A = \left(\frac{\partial F}{\partial R}\right)_{T,N,V}, \tag{3}$$

where $V=As_y$.

If we define interfacial area of the vapor-liquid interface in the simulation box, $A'=2Hs_z$ and $s_x=L$, then a simple mathematical manipulation leads Eq. (3) to

$$\left(\frac{\partial F}{\partial A'}\right) = -\frac{\gamma_2 AL}{Hs_z^2}. \tag{4}$$

Substituting, the value of γ_2, we get a following expression for the surface tension of vapor-liquid under confinement:

$$\left(\frac{\partial F}{\partial A'}\right)_{T,N,V} = \frac{L(p_{xx}-p_{zz})}{2} = \gamma_{v-l}, \tag{5}$$

where p_{xx} is the spreading pressure, parallel to the wall and perpendicular to the interface, and p_{zz} is the pressure component parallel to the interface and parallel to the wall. The division factor of 2 in the above formula accounts for the presence of two interfaces in the system.

To study phase equilibria, we employed GC-TMMC simulation.[20] A detailed information is given by Errington.[20,21] We provide a brief description of the methodology in this section. GC-TMMC simulations are conducted in a grand-canonical ensemble at constant chemical potential μ, volume V, and temperature T. The microstate probability in this ensemble is represented as

$$\pi_s = \frac{1}{\Xi}\frac{V^{N_s}}{\Lambda^{3N_s}N_s!}\exp[-\beta(U_s-\mu N_s)], \tag{6}$$

where $\beta=1/k_BT$ is the inverse temperature and k_B is the Boltzmann's constant, Ξ is the grand partition function, U_s is the interaction energies of particles, and Λ is the de Broglie wavelength. The macrostate probability is calculated by summing all the microstate states at a constant number of molecules N. The mathematical formula can be expressed as

$$\Pi(N) = \sum_{N_s=N} \pi_s. \tag{7}$$

A book keeping scheme of the transition matrix is employed to obtain the macrostate probability. In this scheme, for each MC move we record the acceptance probability in a matrix C, regardless of whether the move is being accepted or not. For example, for a move from a microstate s with N number molecules to a microstate t with M number molecules, the acceptance probability is defined as

$$a(s \to t) = \min[1, \pi_t/\pi_s]. \tag{8}$$

The following recipe is used to update the matrix C:

$$C(N \to M) = C(N \to M) + a(s \to t), \tag{9}$$

and

$$C(N \to N) = C(N \to N) + 1 - a(s \to t). \tag{10}$$

The macrostate transition probability then can be obtained from the matrix C at any time using the following expression:

$$P(N \to M) = \frac{C(N \to M)}{\Sigma_O C(N \to O)}. \tag{11}$$

To obtain the macrostate probabilities, we utilize the following detailed balance expression:

$$\Pi(N)P(N \to M) = \Pi(M)P(M \to N). \tag{12}$$

In the current grand-canonical simulation work, we have employed only deletion, addition, and displacement moves considering one molecule at a time. The possible state change will be from one of the following choices: $N \to N$, $N \to N-1$, and $N \to N+1$, hence the transition probability matrix is tridiagonal. In such conditions, a sequential approach would be an efficient and simple way to obtain the macrostate probabilities,

$$\ln \Pi(N+1) = \ln \Pi(N) - \ln\left[\frac{P(N+1 \to N)}{P(N \to N+1)}\right]. \tag{13}$$

To ensure a uniform sampling across all densities, we have employed multicanonical sampling.[22] This method is applied by assigning each macrostate a weight $\eta(N)$ such that it is inversely proportional to the current estimate of its probability, $\eta(N) = -\ln \Pi(N)$. To remove the bias we need to modify the acceptance criteria as follows:

$$a_\eta(s \to t) = \min\left[1, \frac{\eta(M)\pi_t}{\eta(N)\pi_s}\right], \tag{14}$$

where $\eta(N)$ and $\eta(M)$ are weights corresponding to microstates s and t, respectively. Note that the introduction of a weighting function does not alter the updating mechanism of the collection matrix and the unbiased acceptance probability is still used to update the collection matrix.

At a given coexistence chemical potential, we would observe two peaks in the macrostate probability distribution. However, we usually do not know *a priori* the chemical potential, at which the phase coexistence would occur. To obtain the coexistence chemical potential we have utilized the histogram-reweighting method.[23] This method modifies the probability distribution obtained with the chemical potential μ_0 to μ using the following relation:

$$\ln \Pi(N;\mu) = \ln \Pi(N;\mu_0) + \beta(\mu - \mu_0)N. \tag{15}$$

The coexistence chemical potential is calculated by applying Eq. (15) until we obtain a probability distribution Π_N^{coex} such that area under the vapor and liquid regions in the probability distribution plot are equal. Densities of phases are calculated from the first moment of Π_N^{coex} distribution. The saturation pressure is obtained using the following expression:

$$\beta pV = \ln\left(\sum_N \Pi_N^{\text{coex}}/\Pi_0^{\text{coex}}\right) - \ln(2). \tag{16}$$

The interfacial free energy F_L for a finite-size system with a cell length of L is determined from the maximum likelihood in the liquid ($\Pi_{\max}^l$) and vapor ($\Pi_{\max}^v$) regions and the minimum likelihood in the interface ($\Pi_{\min}$) region,

$$\beta F_L = \tfrac{1}{2}(\ln \Pi_{\max}^l + \ln \Pi_{\max}^v) - \ln \Pi_{\min}. \tag{17}$$

From the formalism of Binder,[17] the interfacial free energy of a two-dimensional surface (with area $A=LH$) varies with system size according to

$$\beta\gamma_L = \frac{\beta F_L}{2A} = C_1\frac{1}{A} + C_2\frac{\ln L}{A} + \beta\gamma_\infty, \tag{18}$$

where γ_L is an apparent system-size-dependent surface tension, γ_∞ is the true infinite-system ($L \to \infty$) interfacial tension, and C_1 and C_2 are constants. The expression suggests that the group $\beta F_L/2A$ becomes linear with the scaling variable $\ln(L)/A$ as the system size approaches infinity. The method enables one to evaluate the infinite-system interfacial tension by extrapolating a series of finite-system interfacial free energies.

III. MODEL AND SIMULATION DETAILS

The simplicity and analytical tractability of the square-well potential besides containing the essential features of attraction and hard repulsion have led to various studies on bulk[24–26] and interfacial properties.[27–29] In this work, the fluid-fluid interaction is represented by the square-well potential,

$$u_{f\text{-}f}(r_{ij}) = \begin{cases} \infty, & 0 < r_{ij} < \sigma \\ -\varepsilon, & \sigma \leqslant r_{ij} < \lambda\sigma \\ 0, & \lambda\sigma \leqslant r_{ij}, \end{cases} \tag{19}$$

where $\lambda\sigma$ is the potential-well diameter, ε is the depth of the well, and σ is the diameter of the hard core. The fluid-wall interaction is also represented by the following square-well-type potential:

$$u_{w\text{-}f}(r) = \begin{cases} \infty, & r < \sigma/2.0 \\ -\varepsilon_{w\text{-}f}, & \sigma/2.0 \leqslant r < \lambda_{w\text{-}f}\sigma \\ 0, & \lambda_{w\text{-}f}\sigma \leqslant r, \end{cases} \tag{20}$$

We adopt units such that ε and σ are unity. In this work, we set $\lambda = 1.5$, $\lambda_{w\text{-}f} = 1.0$, and $\varepsilon_{w\text{-}f}$ was varied from 0 to 4. Reduced units used in this study are temperature $T^* = kT/\varepsilon$, density $\rho^* = \rho\sigma^3$, pressure $P^* = P\sigma^3/\varepsilon$, and surface tension $\gamma^* = \gamma\sigma^2/\varepsilon$.

We have performed MD simulations in a canonical (NVT) ensemble, i.e., at prescribed particle number, volume, and temperature, during equilibration period. The reduced time step Δt^* (in units of $\sigma\sqrt{m/\varepsilon}$) was fixed at 0.04. The temperature was kept constant by simple momentum scaling, with all momenta multiplied by an appropriate factor at the end of each time step such that the total kinetic energy of the system is consistent with the equipartition value of the temperature.[30] The only effect of the time-step parameter is to determine the frequency for updating averages and rescaling velocities to the desired temperature. Once the equilibration period was over, we performed the MD simulation in the microcanonical (NVE) ensemble. The simulations were conducted with the system size of 2000 particles. The total time steps for equilibration and for production were taken as 10^5. Grand-canonical simulations are conducted with 10% dis-

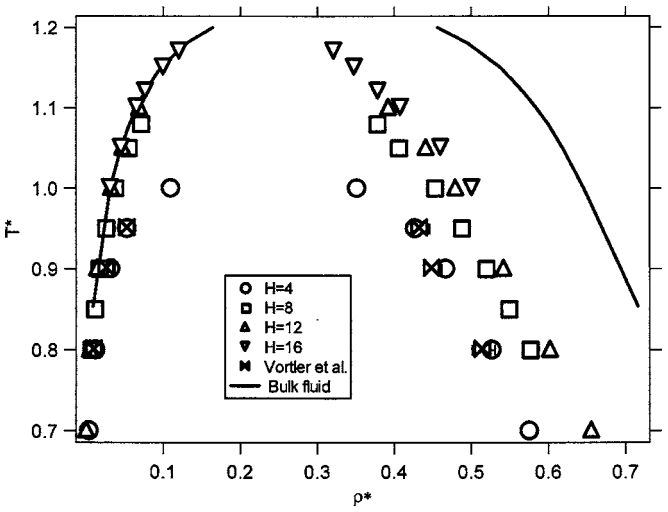

FIG. 1. Temperature-density vapor-liquid coexistence envelope of a SW fluid in a hard planar slit pore of widths ranging from $H=4$ to 16. The phase coexistence densities of the bulk fluid are included in the plot for comparison. The results of Vortler and Smith (Ref. 13) are also included.

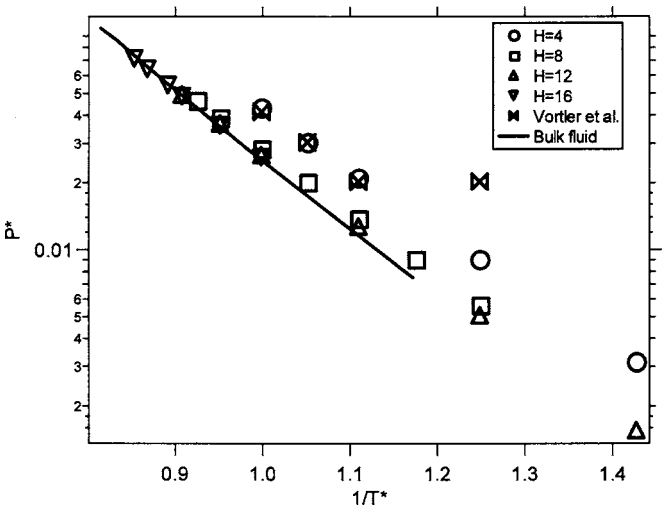

FIG. 2. Vapor pressure of a SW fluid in a hard planar slit pore as a function of the inverse temperature for slit widths ranging from $H=4$ to 16. The solid line represents the saturation pressure of the bulk fluid. The results of Vortler and Smith (Ref. 13) are also included.

placement, 45% insertion, and 45% deletion moves. For the phase coexistence calculation, the box length (all lengths are given in units of the core diameter σ) was varied from $L \sim 5$ to 10 depending on the wall width. To calculate the surface tension using GC-TMMC and finite size scaling, we performed simulations for different box lengths varying from $L \sim 15$ to 30. Four independent runs were conducted to calculate the statistical error.

IV. RESULTS AND DISCUSSIONS

A. Results of hard slit pore

Vortler and Smith[13] used GEMC to obtain the phase coexistence densities of the SW fluid under hard (repulsive) walls. The errors from the GEMC calculation for the vapor density ranged from 14–42% while liquid density errors were in the range of 2%–3%. They also show that the free energy perturbation (FEP) technique along with the integration of the Gibbs-Duhem (GD) equation yields similar results; however, the error estimate for the vapor phase is much higher than that from the GEMC approach. For slit width $H=4$, our values are in good agreement with their GEMC results as shown in Fig. 1. In comparison to GEMC and FEP+GD, GC-TMMC shows superior estimates of the phase coexistence values under confinement in terms of accuracy and performance. Errors via GC-TMMC were less than 0.1% for phase densities and the saturation pressure. At $H=4$, the liquid density is found to be considerably lower than the value of bulk fluid. At a constant temperature, an increase in the slit width causes the increase of the saturation liquid density and the decrease of the saturation vapor density. The effect of confinement is exerted more on liquid phase than vapor phase, as evident from Fig. 1, where we observe the agreement of saturation vapor density at various slit widths, for certain range of temperatures, with that of saturated bulk (unconfined) vapor phase. It is known that the critical temperature would get suppressed under the presence of walls.[3,31] In this work we have used the rectilinear diameter approach[13] to calculate the critical properties, which are reported in Table I. The critical temperature decreases with the decrease in the slit width. A similar behavior is being observed for the critical pressure. The critical density appears to be relatively insensitive to the variation in the slit width.

Figure 2 presents the results of the saturation pressure against the inverse temperature in a Clausius-Clapeyron plot. Our results are in good agreement with the data of Vortler and Smith except for the lower temperature. The severe deviation may come from the inaccurate prediction from the FEP+GD approach at low temperature range, where the large error is generally persistent. The saturation pressures

TABLE I. The critical temperature T_c^*, density ρ_c^*, and pressure P_c^* data of a square-well fluid in a planar slit pore of variable slit width H and different wall-fluid interactions estimated from the GC-TMMC and rectilinear diameter approaches. Numbers in parentheses indicate the 67% confidence limits of the last digit of the reported value.

	Hard wall			Attractive wall, $H=8$			
H	T_c^*	ρ_c^*	P_c^*	$\varepsilon_{w\text{-}f}$	T_c^*	ρ_c^*	P_c^*
4	1.015(1)	0.2265(2)	0.045(6)	1	1.153(4)	0.2599(7)	0.073(2)
8	1.143(3)	0.2101(6)	0.0635(7)	2	1.167(3)	0.3109(7)	0.106(1)
12	1.177(3)	0.2143(5)	0.0720(5)	3	1.132(3)	0.3834(8)	0.163(2)
16	1.201(8)	0.2082(45)	0.0818(30)	4	1.121(7)	0.4201(4)	0.274(2)

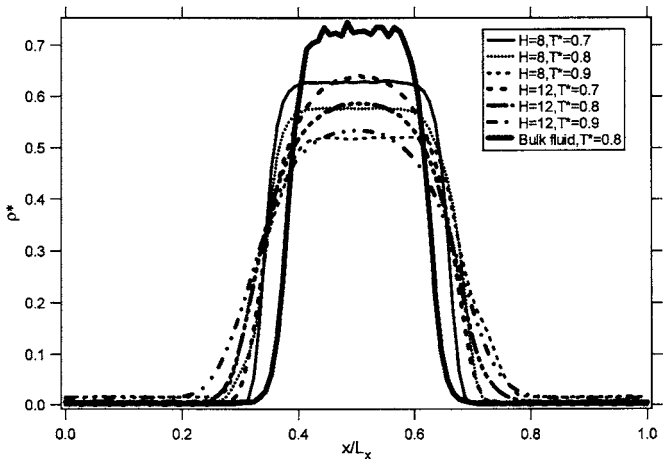

FIG. 3. Vapor-liquid density profile of a SW fluid in a hard planar slit pore of width $H=8$ and 12 at temperature from $T^*=0.7$ to 0.9. The abscissa is the reduced length of the x axis (parallel to the walls) of the simulation box. Density profile of the bulk fluid, at $T^*=0.8$, is also plotted for reference.

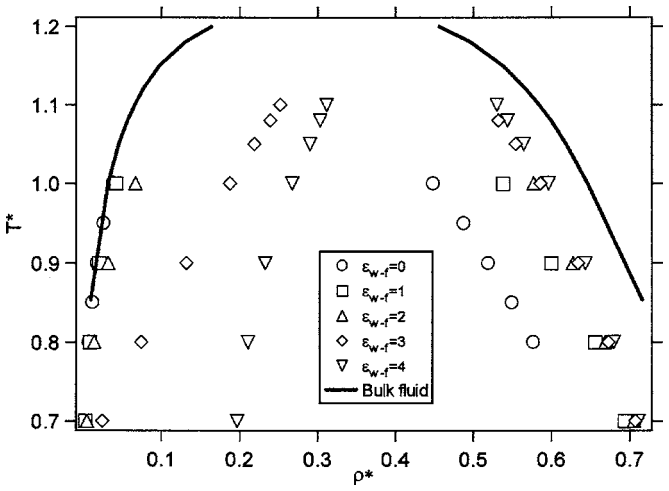

FIG. 5. Vapor-liquid phase coexistence densities of a SW fluid in an attractive planar slit pore of width $H=8$ for various temperatures. The phase coexistence density of the bulk fluid is included in the plot for comparison. $\varepsilon_{w\text{-}f}=0$ represents the hard wall-fluid interaction energy.

under the slit pore confinement are generally higher than the bulk saturation ones. The pressures accordingly decrease as the slit width increases and reach to the bulk saturation pressures at $H=12$. At a constant subcritical temperature, we observe that a further increase in the slit width results in no change in the saturation pressure.

The density profile qualitatively reveals the important information about the thickness of the vapor-liquid interface and the surface tension. Figure 3 shows the density profile of the SW fluid under hard slit widths of 8 and 12 for a temperature range from 0.7 to 0.9. The density profile of the bulk fluid[29] at $T^*=0.8$ is included in the figure for reference. The interfacial width (data not shown) increases with the increase of the temperature for a constant wall width. However, for a given temperature, the interfacial width decreases with the increase of the wall width, qualitatively indicating that the vapor-liquid surface tension increases with increasing wall width.[32] Beyond $H=12$, we expect a gradual increase of the surface tension as the wall width increases. The results are shown in Fig. 4. The surface tension[29] of the bulk vapor-liquid SW fluid is plotted for the reference. The values of the vapor-liquid surface tension of the confined SW fluid are significantly lower than the bulk surface tension values over the wall width of interest. For example at $T^*=1.0$, the bulk vapor-liquid surface tension is 0.280 ± 0.004 and the confined surface tension value for $H=4$ is 0.025 ± 0.001, which is around ten times lower. This significant reduction of the surface tension is attributed to the reduction in the surface free energy due to confinement.

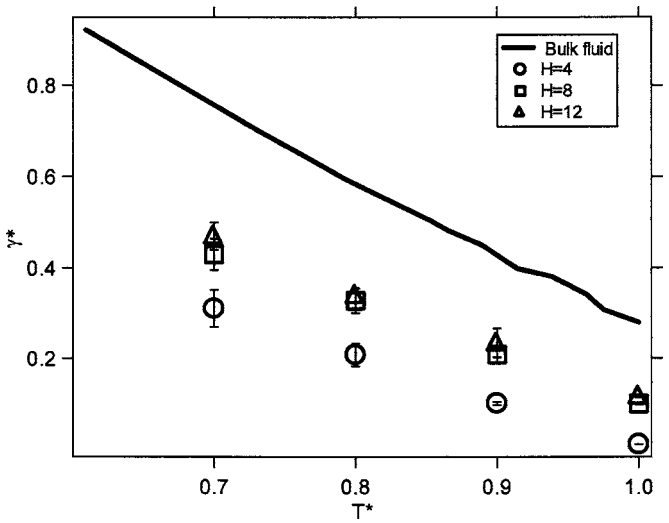

FIG. 4. Vapor-liquid surface tension of a SW fluid in a hard planar slit pore against temperature for various slit widths.

B. Results of attractive slit pore

In this section, we present the effects of the attractive walls on the SW fluid. Figure 5 presents the vapor-liquid phase coexistence densities of a SW fluid in an attractive planar slit pore of width $H=8$ for various attractive wall-fluid interaction energies. A rise in the liquid density and vapor density is observed with the increase in the wall-fluid interaction. The vapor phase experiences significant structural changes as the wall-fluid interaction is increased from $\varepsilon_{w\text{-}f}=2$ to 4, which is reflected by the *shift* in the density. The liquid density, however, does not behave in a similar fashion for the case of change from $\varepsilon_{w\text{-}f}=2$ to 4. To understand this sudden shift in the vapor density we seek the explanation from the vapor density profile for those wall-fluid interactions at $T^*=0.9$. Figure 6 shows the results obtained from simple vapor phase MD simulations. An interesting behavior is observed as the wall-fluid interaction is changed from $\varepsilon_{w\text{-}f}=2$ to 3. A second layer of fluid (near the wall), in the vapor phase, appears for the case of $\varepsilon_{w\text{-}f}=3$, which, we believe, mainly causes the sudden increase of the vapor density as noticed in Fig. 5. A further increase in the wall-fluid interaction, from $\varepsilon_{w\text{-}f}=3$ to 4, increases the densities of fluid in the first and second layers near the wall. Therefore, the average density of the vapor phase further increases.

The saturation pressures for different attractive wall-fluid interactions at a constant slit width, $H=8$, are plotted along with bulk saturation pressure in Fig. 7. The saturation

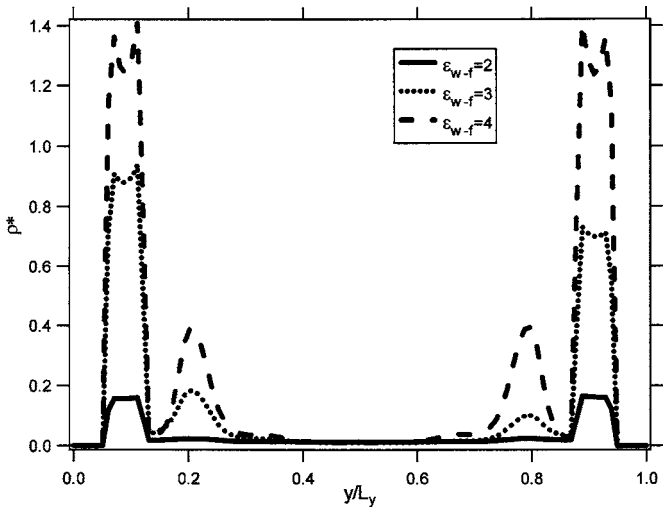

FIG. 6. Density profile of vapor phase of a SW fluid in an attractive planar slit pore of width $H=8$. The abscissa is the reduced length of the y axis (perpendicular to the walls) of the simulation box. The peaks close to the walls represents the layering of particles.

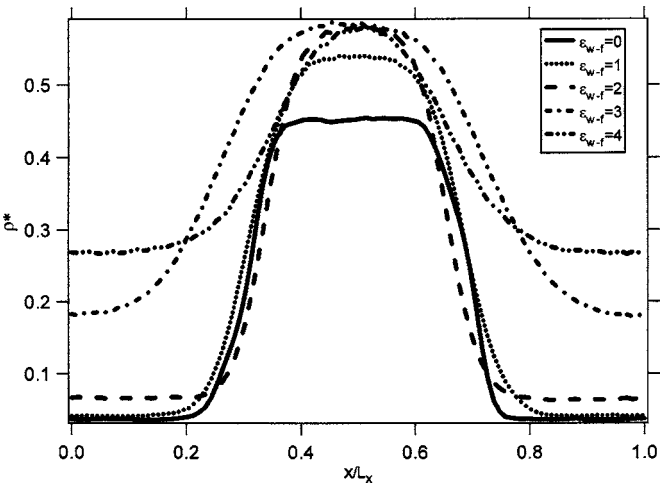

FIG. 8. Vapor-liquid density profile of a SW fluid in an attractive planar slit pore of width $H=8$ at $T^*=1.0$. The abscissa is the reduced length of the x axis (parallel to the walls) of the simulation box. The density profile of the SW fluid under the hard repulsive wall, at $T^*=1.0$, is also included for reference.

pressure increases with the increase in the wall interaction. The change in the saturation pressure is significant which increases more than 30-fold as we change the wall-fluid interaction from $\varepsilon_{w\text{-}f}=2$ to 4 at $T^*=0.7$. At the high temperature region, the change in the wall-fluid interaction, as above, lead to only about a fivefold increase in the saturation pressure. Figure 8 shows the density profile for different attractive wall-fluid interactions. We observe an interesting phenomenon on the interfacial thickness, which shows a minimum with respect to the change in the wall-fluid interaction. The thickness (calculation not shown) first decreases then it starts increasing with the increase in the wall-fluid interaction. The weak wall fluid ($\varepsilon_{w\text{-}f}<2$) affects the liquid phase more than the vapor phase. The liquid phase allows a higher density region near the wall relative to the vapor phase. Hence with the increase in the wall-fluid interaction molecules, in the liquid phase, tend to accumulate near the wall causing a layering behavior. This in effect increases the average liquid phase density (see Fig. 5) whereas the absence of the layering behavior leads to an insignificant effect on the vapor phase. Due to the above we observe a decrease in the interfacial thickness or increase in the sharpness of the interface. However, with the further increase in the wall-fluid interaction ($\varepsilon_{w\text{-}f}>2$) the effect is now more on the vapor phase with molecules near the wall now representing the same kind of structure (see Fig. 6) as found in the liquid phase. This led to the increase in the vapor density as shown in Figs. 5 and 8. The liquid phase average density also increases though now not as dramatic as was the case for $\varepsilon_{w\text{-}f}=1$. The surface tension for a constant slit width and temperature increases till $\varepsilon_{w\text{-}f}=2$ as shown in Fig. 9. The increment in the surface tension can be attributed to the increase in the surface excess free energy. Since the weak interaction favors the liquid phase more as compared to the vapor phase, the associated free energy change from liquid to the interface or from interface to the vapor phase increases till $\varepsilon_{w\text{-}f}=2$ hence the rise in the surface tension. On the other

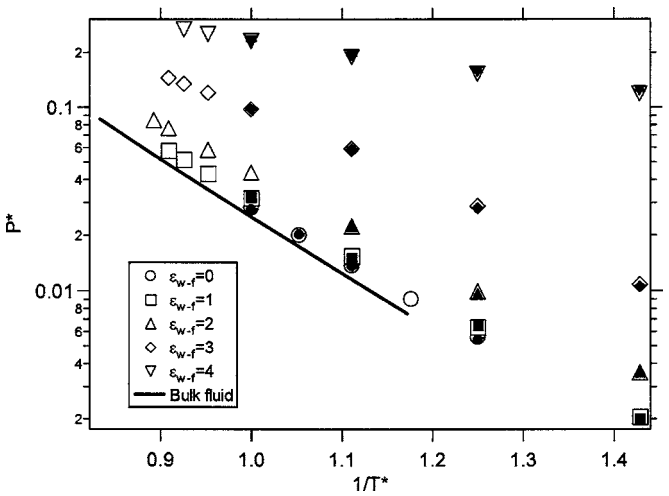

FIG. 7. Clausius-Clapeyron plot of vapor pressure of a SW fluid in an attractive planar slit pore of width $H=8$. Filled symbols are MD results.

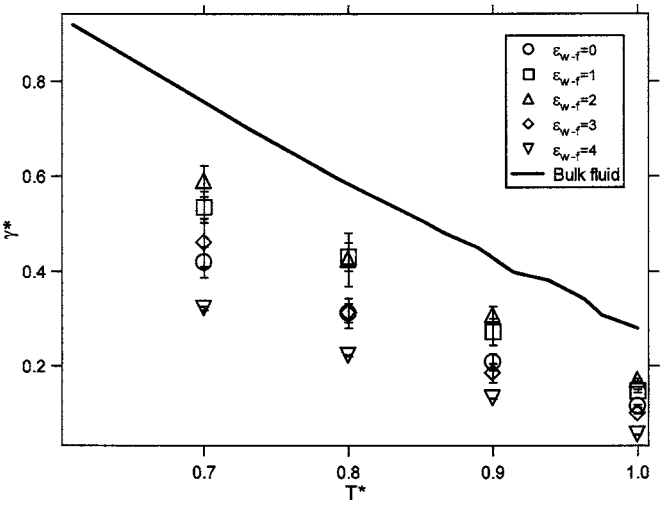

FIG. 9. Vapor-liquid surface tension, as a function of temperature, of a SW fluid in an attractive planar slit pore of width $H=8$.

TABLE II. Surface tension data of square-well molecules confined in a planar slit pore of width $H=8$ of varying system size (nonconfined sides of length L, in units of σ) from the grand-canonical transition-matrix Monto Carlo and comparison with values from MD simulations. $T^*=kT/\varepsilon$. Numbers in parentheses indicate the 67% confidence limits of the last digit of the reported value.

T^*	$L=15$	$L=17$	$L=20$	$L=25$	$L=30$	$L=\infty$	MD
0.80	0.3146(2)	0.3157(19)	0.3159(24)			0.323(16)	0.329(23)
0.90	0.2025(9)	0.2021(11)	0.2021(21)	0.2040(32)	0.2075(37)	0.222(15)	0.208(16)
0.95	0.1507(2)	0.1513(4)	0.1505(11)	0.1506(9)	0.1509(18)	0.152(7)	0.156(6)
1.00	0.1019(2)	0.1024(3)	0.1021(1)	0.1017(5)	0.0990(13)	0.096(3)	0.102(3)

hand, at $\varepsilon_{w\text{-}f}=3$, the first layer is firmly formed and the second layer starts to form in the vapor phase region. The attractive force of these layers of particles around the interface causes to attract some particles from both phases, hence a broader density profile is observed. At $\varepsilon_{w\text{-}f}=4$, the layering effect in the liquid phase saturates, and hence there is hardly any more increase in the average liquid density. On the contrary the layering effect still continues to increase the average vapor density and diminishing the structural difference between vapor and liquid phases. This results in the narrowing of the body of the "bell" shaped curve in the density profile. We speculate that the layering effect will be the dominant factor beyond this wall-fluid interaction. The effect of the higher wall-fluid interaction on the surface tension is also shown in Fig. 9 which shows that beyond $\varepsilon_{w\text{-}f}=2$ the surface tension decreases. This decrease in the surface tension can also be attributed to the decrease in the surface excess free energy. This trend similarly occurred at different temperatures. Critical properties for the SW fluid in the attractive planar slit pore are presented in Table I. The critical temperature exhibits a maximum, similar to the surface tension behavior, with respect to wall-fluid interaction. However, the critical density linearly increases with the wall-fluid interaction whereas the critical pressure exponentially increases with the wall-fluid interaction.

Finite size scaling (FSS) of the Binder formalism[17] is not a customary method to calculate the surface tension. However, it has been shown[29] that GC-TMMC incorporated with FSS can be a very effective method, in particular, near critical temperature, where slab based methods can be difficult to perform due to an unstable interface (which essentially will require the system size to increase). Errington[21] utilized finite-system size surface tension values corresponding to a cubic box length ranging from $L=9$ to 14 for the three-dimensional nonconfined system of the Lennard-Jones fluid to obtain the surface tension of the infinite system size. The maximum number of molecules for the system was around 2500 corresponding to $L=14$. GC-TMMC with FSS has also been applied to study the surface tension of chain molecules[33] where it was found that scaling is sufficient if the system size is varied from 900 to 2100 molecules. In the present work, we studied the system size (maximum number of molecules) from 1100 ($L=15$) till 4000 ($L=30$) except for the case of $T^*=0.8$ where the maximum number of molecules considered was 2100 corresponding to $L=20$. Table II presents the results of GC-TMMC with the FSS study of the slit width, $H=8$. The results of MD simulations are also listed in Table II for comparison. Surface tension values from the GC-TMMC-FSS study are in good agreement with MD results.

V. CONCLUSIONS

We have determined the phase behavior and the surface tension of liquid-vapor phases of a SW fluid confined between infinite planar walls of an attractive as well as a repulsive nature. The GC-TMMC technique is demonstrated for calculating phase equilibria of confined fluids and we have shown this to be more accurate in comparison to the GEMC and FEP+GD techniques used by Vortler *et al.*[13] Besides the phase coexistence, the surface tension is also calculated by using the finite-size technique of Binder[17] and compared with outcomes from a MD simulation. The results are generally in good agreement. The surface tension of the vapor-liquid SW fluid under slit pore confinement is comparatively very low with respect to the bulk vapor-liquid surface tension due to the reduction of the surface excess free energy. The effect is more pronounced for the case of attractive walls, where the surface tension slightly increases with the increase in the wall-fluid interaction. However, once the wall-fluid interaction is stronger than the fluid-fluid interaction, the surface tension drops below the surface tension value of the vapor liquid under hard walls.

ACKNOWLEDGMENTS

Computational resources have been provided by the Computer Center at the Indian Institute of Technology Kanpur and the School of Chemical and Biomedical Engineering at Nanyang Technological University, Singapore.

[1] R. Evans, J. Phys.: Condens. Matter **2**, 8989 (1990).
[2] R. Evans and A. O. Parry, J. Phys.: Condens. Matter **2**, SA15 (1990).
[3] L. D. Gelb, K. E. Gubbins, R. Radhakrishnan, and M. Sliwinska-Bartkowiak, Rep. Prog. Phys. **62**, 1573 (1999).
[4] A. Z. Panagiotopoulos, Mol. Phys. **61**, 813 (1987).
[5] D. A. Kofke, Mol. Phys. **78**, 1331 (1993).
[6] D. Moller, J. Oprzynski, A. Muller, and J. Fischer, Mol. Phys. **75**, 363 (1992).
[7] D. Moller and J. Fischer, Mol. Phys. **69**, 463 (1990).
[8] A. Lofti, J. Vrabec, and J. Fischer, Mol. Phys. **76**, 1319 (1992).
[9] A. Z. Panagiotopoulos, Mol. Phys. **62**, 701 (1987).
[10] L. Sarkisov and P. A. Monson, Phys. Rev. E **61**, 7231 (2000).
[11] J. Forsman and C. E. Woodward, Mol. Phys. **90**, 637 (1997).
[12] W. R. Smith and H. L. Vortler, Chem. Phys. Lett. **249**, 470 (1996).
[13] H. L. Vortler and W. R. Smith, J. Chem. Phys. **112**, 5168 (2000).
[14] B. Widom, J. Chem. Phys. **39**, 2808 (1963).
[15] R. Eppenga and D. Frenkel, Mol. Phys. **52**, 1303 (1984).

[16] H. Zhang, B.-J. Zhang, J. Lu, and S. Liang, Chem. Phys. Lett. **366**, 24 (2002).
[17] K. Binder, Phys. Rev. A **25**, 1699 (1982).
[18] D. J. Diestler, M. Schoen, J. E. Curry, and J. H. Cushman, J. Chem. Phys. **100**, 9140 (1994).
[19] D. J. Diestler, J. Phys. Chem. **100**, 10414 (1996).
[20] J. R. Errington, J. Chem. Phys. **118**, 9915 (2003).
[21] J. R. Errington, Phys. Rev. E **67**, 012102 (2003).
[22] B. A. Berg and T. Neuhaus, Phys. Rev. Lett. **68**, 9 (1992).
[23] A. M. Ferrenberg and R. H. Swendsen, Phys. Rev. Lett. **61**, 2635 (1988).
[24] F. Del Rio and D. A. Delonngi, Mol. Phys. **56**, 691 (1985).
[25] L. Vega, E. de Miguel, L. F. Rull, G. Jackson, and I. A. McLure, J. Chem. Phys. **96**, 2296 (1992).
[26] F. del Rio, E. Avalos, R. Espindola, L. F. Rull, G. Jackson, and S. Lago, Mol. Phys. **100**, 2531 (2002).
[27] P. Orea, Y. Duda, and J. Alejandre, J. Chem. Phys. **118**, 5635 (2003).
[28] G. J. Gloor, G. Jackson, F. J. Blas, and E. De Miguel, J. Chem. Phys. **123**, 134703 (2005).
[29] J. K. Singh, D. A. Kofke, and J. R. Errington, J. Chem. Phys. **119**, 3405 (2003).
[30] M. P. Allen and D. J. Tildesley, *Computer Simulation of Liquids* (Clarendon, Oxford, 1987).
[31] R. Evans, M. B. Marconi, and P. Tarazona, J. Chem. Phys. **84**, 2376 (1986).
[32] T. B. Peery and G. T. Evans, J. Chem. Phys. **114**, 2387 (2001).
[33] J. K. Singh and J. R. Errington, J. Phys. Chem. B **110**, 1369 (2006).